ORIGINAL PAPER

Light activation of the isomerization and deprotonation of the protonated Schiff base retinal

**Carlos Kubli-Garfias · Karim Salazar-Salinas ·
Emily C. Perez-Angel · Jorge M. Seminario**

Abstract We perform an *ab initio* analysis of the photo-isomerization of the protonated Schiff base of retinal (PSB-retinal) from 11-*cis* to 11-*trans* rotating the C10-C11=C12-C13 dihedral angle from 0° (*cis*) to -180° (*trans*). We find that the retinal molecule shows the lowest rotational barrier (0.22 eV) when its charge state is zero as compared to the barrier for the protonated molecule which is ~0.89 eV. We conclude that rotation most likely takes place in the excited state of the deprotonated retinal. The addition of a proton creates a much larger barrier implying a switching behavior of retinal that might be useful for several applications in molecular electronics. All conformations of the retinal compound absorb in the green region with small shifts following the dihedral angle rotation; however, the Schiff base of retinal (SB-retinal) at *trans*-conformation absorbs in the violet region. The rotation of the dihedral angle around the C11=C12 π-bond affects the absorption energy of the retinal and the binding energy of the SB-retinal with the proton at the N-Schiff; the binding energy is slightly lower at the *trans*-SB-retinal than at other conformations of the retinal.

C. Kubli-Garfias · K. Salazar-Salinas · E. C. Perez-Angel ·
J. M. Seminario (✉)
Department of Chemical Engineering, Texas A&M University,
College Station, TX, USA
e-mail: seminario@tamu.edu

C. Kubli-Garfias · K. Salazar-Salinas · E. C. Perez-Angel ·
J. M. Seminario
Department of Electrical and Computer Engineering,
Texas A&M University,
College Station, TX, USA

C. Kubli-Garfias
Instituto de Investigaciones Biomédicas,
Universidad Nacional Autónoma de México,
México, DF, Mexico

Introduction

Light plays a vital role in many biological systems. For instance, photosynthesis in plants, vision in animals, communication in protozoa and bacteria [1, 2], orientation and migration of microorganisms by phototaxis [3], acceleration of biochemical reactions and transduction processes that trigger ultrafast initial events by promoting conformational changes on enzymes previous to catalysis [4], activation by ultraviolet radiation of photoreaction of provitamin D_3 [5], and a large amount of other examples.

On the other hand, rhodopsin, the most conspicuous protein in vision, has been studied extensively and its light transduction phenomena have already been biochemically described [6]. Rhodopsin is bonded to a retinal chromophore; the initial step of the visual signal transduction is the isomerization of the 11-*cis*-protonated Schiff base retinal (11-*cis*-PSB-retinal) by light energy absorption [7]. The photon absorption of 11-*cis*-PSB-retinal promotes a conformation change toward the *trans*-PSB-retinal form, including similarly, deprotonation of the Schiff base at the side chain of Lysine296. The very early stage of the photocycle in retinal is the isomerization of the C11-C12 π-bond with smaller changes of other torsion angles distributed over the length of the conjugated chain. Regarding the possible isomerizations, the following mechanisms have been reported for retinal:

(a) The single bond rotation whereby only the rotation of the C11=C12 double bond is considered, but the twisting of 40°, for instance, it is enough to change

some properties such as adiabatic potentials, absorption wavelengths and dipole moments, in addition to the geometry [8].

(b) The bicycle pedal-like, which is a progressive *cis-trans* isomerization cascade of the polyene chain toward the isoprenoid tail, yields the all-*trans* isomer. In addition, an all *trans* retinal intermediate is produced from the 11-*cis*, 12-s *trans* conformation [9].

(c) The hula-twist method, which consists in the simultaneous twisting of a pair of adjacent isomerizable π- and σ-bonds rotating somehow in opposite directions. Twist of C10-C11 and C12-C13 bonds in the same direction [10]. Unlike the bicycle pedal, the hula twist changes its direction because the bond twisting. This may occur in different types of polyenes.

(d) The twist sharing model, in which the isomerizable double bond (C11=C12) and single bonds rotate somehow in opposite directions. In this model, the C11=C12 bond rotates counterclockwise while the contiguous C9=C10, C10-C11 and C12-C13, C13=C14 rotate clockwise in opposite direction [11].

(e) The asynchronous bicycle-pedal or crankshaft, also more properly, asynchronous crankshaft coordinate [12, 13], in which the -C9=C10- and -C11=C12- bonds rotate in opposite directions as in the twist sharing model, but the -C9=C10- bond is blocked when the 19-methyl group interacts with the surrounding aminoacids of rhodopsin [11].

However, first principles studies of the transduction mechanisms remain unexplored, *e.g.*, effects such as phononic, photonic, and tunneling in the photoactivation of biomolecules [14, 15]. In this work, we describe the single rotation around the C11=C12 bond by first principles calculations.

Methodology

Biological model: retinal chromophore bonded to rhodopsin protein

The apoprotein pocket, a polypeptide chain that binds to its specific prosthetic group, plays an important role in the stabilization of the retinal structure. Retinal can twist around its double bonds by the absorption of photon energy. This twisting is self-controllable due to the steric interaction of the retinal methyl groups with the protein environment [16]. For instance, the Trp265 remains stabilized in the *cis*-retinal conformation because the steric constraint exerted upon the C20 methyl group of the retinal [17]. When this constrain disappears and the *trans*-PBS-retinal is formed, the C20-Trp265 contact changes to C19-Trp265 [18, 19]. The protein

also has a counterion switch that neutralizes the PSB-retinal during its photoisomerization (*cis-trans*). In dark conditions, the positive charge of the 11-*cis*-PSB-retinal is neutralized by Glu113 and by Glu181 when the all-*trans*-PSB-retinal is present (after light exposition) [20]. Figure 1 shows the framework formed by rhodopsin (cartoon format) and its ligand retinal (light blue residue in licorice format).

The photoisomerization of the retinal into the rhodopsin protein is faster (less than 200 fs) than the non bonded retinal (several ps) [21] because the steric interaction [22, 23] and rotating moment between electric dipole moments of methyl groups of PSB-retinal can promote fast isomerization upon light absorption [24]. After the photoisomerization, the methyl groups and the β-ionone ring are reoriented and lead the deprotonation of the Schiff base causing the H-bond network disruption among the Trp265, Phe261, Tyr268 and Glu181 residues (Fig. 2). Even far from the retinal moiety, there is an important interhelical ionic lock composed by Arg135-Glu134 and Arg135-Glu247, which are modified by the retinal isomerization due to the displacement of the flexible helix-6 [25, 26]. However, the connection between the protonation/deprotonation of the ionic lock to the protonation/deprotonation of the Schiff base linkage is still unclear [27].

We approach the biological photoelectric phenomena that takes place in rhodopsin from an atomistic first principles theory applied to several kinds of related systems reported elsewhere [28–30], i.e., density functional theory
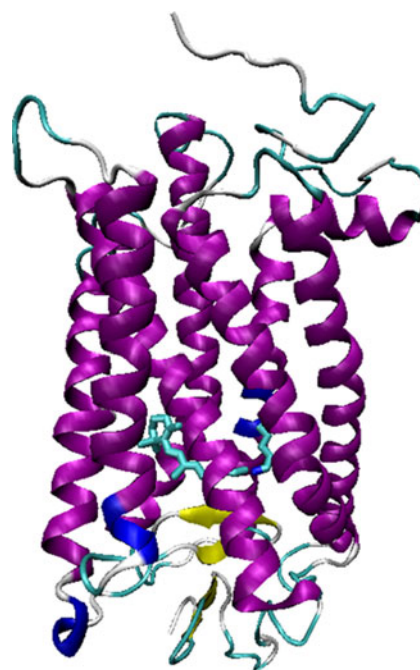

Fig. 1 The retinal chromophore bonded to rhodopsin, which is composed of seven-transmembrane α-helices (PDB code, 1U19). Colors encode the secondary structure of the protein
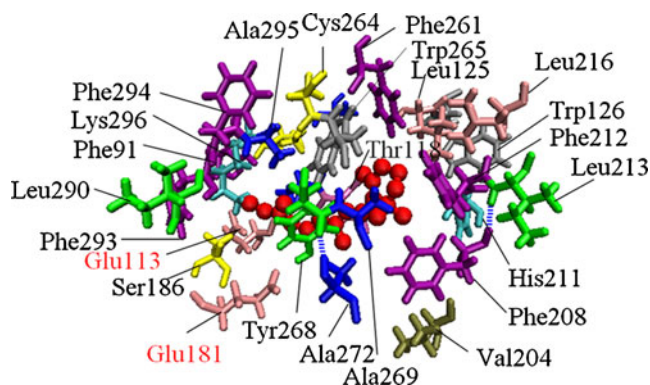
Fig. 2 Partial view of the aminoacid pocket surrounding the retinal with the protonated Schiff base of Lys296 in rhodopsin (1U19, PDB). Retinal is in CPK form (red) and the aminoacids are color-encoded: Lysine296 (blue), Glutamic acid 113 and 181 (red), also H-bonds (dashed blue bars)

(DFT). Then, followed by a time-dependent DFT (TD-DFT). A better understanding of biomolecules allows us to propose them in sensors as explained in [31–34]. Thus we perform *ab initio* calculations using DFT [35–37] and TD-DFT [38] using the *GAUSSIAN-03* [39] and *GAUSSIAN-09* [40] programs. The energy of the PSB-retinal and SB-retinal isomers are minimized in order to get local minima using the hybrid B3PW91 functional [26, 41–43] and the 6-31+G(d) Pople's basis set, which was constructed by adding diffuse s and p functions to the standard 6-31G(d) basis set [44–46]. These methods have been widely tested in several types of systems from molecular electronics [28–30, 47–53], catalysis [54–57], energetic materials [58–64] to biological systems [32, 33] yielding acceptable results very close to chemical accuracy when they are compared to available experimental results [65].

We calculate the ground state and the vertical excitation energy of the PSB-retinal isomers, rotating the C11=C12 double bond of retinal which includes the protonated Schiff base (Fig. 3). The rotation is carried out in steps of 10° from 0°-180° to the dihedral angle C10-C11=C12-C13, fixing the four atoms at each angle to maintain the dihedral. The absorption spectrum is characterized by the vertical
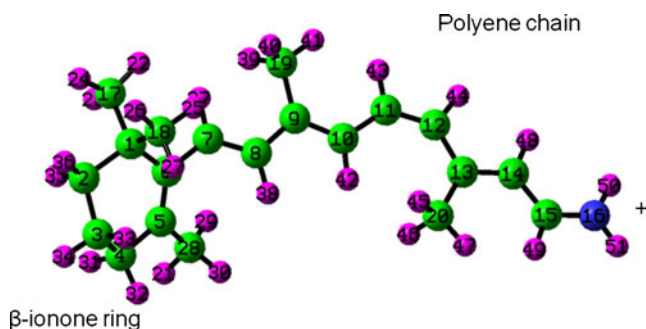

Fig. 3 Protonated Schiff base (PSB) of retinal structure bonded to Lys296 in dark condition. Rotational dihedral angle: C10-C11=C12-C13

Table 1 Optimized structure total energies (hartrees) of the *cis* and *trans* conformations (with respect to the C10-C11=C12-C13 dihedral angle) of PSB-retinal and their energy difference (kcal mol⁻¹)

Compound	Energy	C10-C11=C12-C13 dihedral angle
11-*cis*-PSB-retinal	-834.40046 Ha	0.09°
all-*trans*-PSB-retinal	-834.40783 Ha	-179.88°
energy difference	4.96 kcal/mol	

excitation energies, which are calculated by the TD-DFT at each point of the rotation interval.

Results and discussion

This photoisomerization study of the retinal compound includes the ground state and the first vertical excited state analyzed at each retinal conformation in steps of 10° rotations around the C11=C12 bond constraining the positions of atoms 10, 11, 12, 13 (Fig. 3) to be fixed and allowing all others to relax toward a minimum energy. The constraining of the atoms is done in order to obtain faster results as all these calculations are computationally demanding. Later on, we perform optimizations keeping just the dihedral between two planes of atoms fixed and allowing all other coordinates of the four central atoms and all other atoms of retinal to relax during the energy minimization. Comparison of constrained and unconstrained results does not show large differences (vide infra).

Ground state (S₀) of protonated Schiff base retinal (PSB-retinal): The PSB-retinal is found more stable at the all-*trans*-retinal conformation. Its energy difference with respect to 11-*cis*-PSB-retinal is 4.96 kcal mol⁻¹ (Table 1). The isomerization of PSB-retinal from 11-*cis*- to all-*trans*-retinal shows a transition state (TS) when the rotation around C11=C12 bond reaches 90°. The imaginary frequency at 90° (C10-C11=C12-C13 dihedral) corroborates the transition state of this isomer; its energy difference with respect to all-*trans*-PSB-retinal is 1.01 eV. Besides, it shows the lowest HOMO-LUMO gap (2.04 eV).

Also the C=C bond stretching mode is very intense in the all-*trans*-PSB-retinal isomer. Table 2 and Fig. 4 show the small upshift of the C=N vibration, which means that the

Table 2 Infrared frequencies of the 11-*cis*-, transition state, and all-*trans*-PSB-retinal. Stretching modes (ν). Frequency values are in cm⁻¹

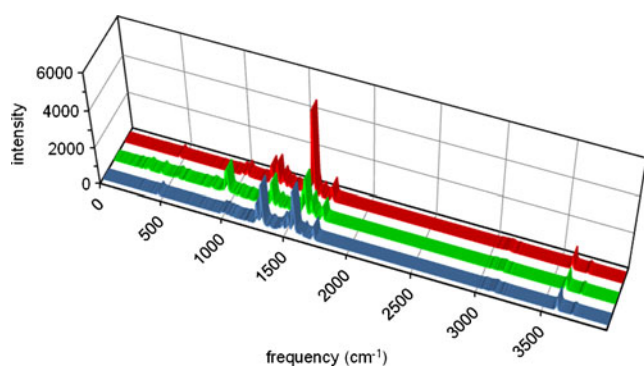| Mode	11-*cis*-PBS-retinal	TS-PSB-retinal	all-*trans*-PBS-retinal
ν(C=C)	1563	1581	1567
ν(C=N)	1717	1717	1718
ν(N-H)	3601	3608	3601

Fig. 4 Infrared spectra of the 11-*cis*-, transition state-, and all-*trans*-PSB-retinal at ground state. ■ 11-*cis*-PSB-retinal ■ TS-PSB-retinal ■ all-*trans*-PSB-retinal

isomerization of C11=C12 does not affect the C=N bond length. There is a downshift of the C=C stretching frequencies among the isomers, indicating the lower bond order of C=C.

The molecular orbital analysis at ground state corroborates that the electronic structures of the PSB retinal-conformers are delocalized mainly at the polyene chain (Fig. 5). The shape and location of the frontier orbitals is similar among the retinal conformations with the exception of the PSB-retinal with dihedral angle of 80° (not shown). In this case, the HOMO populates the end of the polyene chain while it is absent in the methyl groups of the β-ionone ring.

There is an enhancement in the density of states (DOS), at around -14 eV (Fig. 6). This is actually the region that embraces most of the changes in the spectrum due to rotation of the dihedral C10-C11=C12-C13. The highest peaks in the DOS for 11-*cis*- and all-PSB-*trans*-retinal are at the same level of energy (-14.04 eV); however, the transition state shows a shift to -13.52 eV due to the rotation around C11=C12 bond. Thus, we suggest that the electrons located around the energy range (-14.02 to -13.52 eV) are affected by the torsion of the C11=C12 bond.

Vertical excited state (S$_v$) of protonated Schiff base retinal (PSB-retinal): The isomerization from 11-*cis*- to all-*trans*-PSB-retinal promoted by the photon energy yields conformational changes causing electron density rearrangements. The PSB-retinal isomers simulating the rotation of the dihedral angle yield excitation energies from the singlet ground state (S$_0$) to the lowest singlet vertical excited state (S$_v$), from 2.18 to 2.36 eV (Fig. 7a).
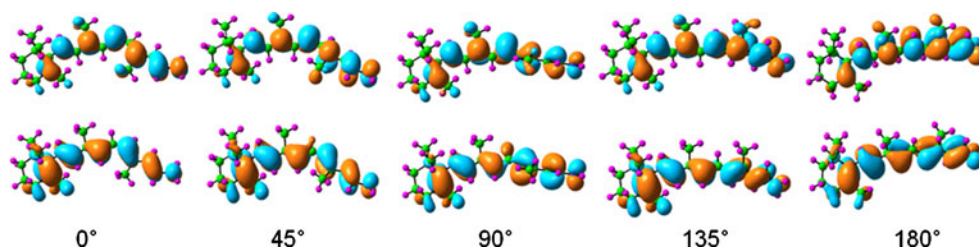
The lowest energy absorption occurs during the C11=C12 torsion at 90° (transition state) and the highest at 180° (all-*trans*-retinal-PSB-retinal), similar to the results reported in [66]. The curves we obtained are slightly asymmetrical, with slightly higher excitation when the dihedral angle approaches to the all-*trans*-PSB-retinal conformation (Fig. 7b).

The vertical excitation of the PSB-retinal causes electron excitations from HOMO to LUMO. However, this simple analysis is insufficient to predict the absorption energy of a compound at S$_0$ by just considering the HOMO-LUMO gap energy, because there are other contributions due to the multi-determinant nature of the wavefunction.

Table 3 shows the contribution of each particle-hole pair by a set of coefficients. All the isomers show a maximum absorption at the green region. It shows a maximum oscillator strength (1.46) when the dihedral angle C10-C11=C12-C13 is at 80°.

The first vertical excited stated for the isomers with dihedral angles of 80°-100° includes only $\psi_{HOMO} \rightarrow \psi'_{LUMO}$ transitions (Table 3), corresponding to the lowest absorption energy; whereas for isomers with other orbital contributions, the absorption increases in energy to extreme values, i.e., when the dihedral angle is approaching values of 0° or 180°. The isomers with dihedral angles of 0°, 10°, 60°, 70°, 170°, 180° and 210° involve excitations into the ψ'_{LUMO}, resulting in significant contributions from both ψ_{HOMO-1} and ψ_{HOMO}. In contrast, the excited states for the isomers with dihedral of 20°-50° and 110°-160° lead to weak transitions.

The vertical transition energy of 11-*cis*-PBS-retinal of 2.30 eV, calculated at the TD-B3PW91/6-31+G(*d*) level, is close to the one reported at the CASPT2//MP2 level of 2.28 eV [67] and for the all-*trans*-PSB-retinal, our result of 2.35 eV is also close to the TD-B3LYP/6-31G(*d*) [68]. Upon the vertical excitation of the PSB-retinal isomers, the S$_v$ state has a dominant hole-pair (ionic) character, similar to that reported in [69].

There are significant changes in the transition dipole moment magnitude due to the isomerization from the 11-*cis*- to all-*trans*-PSB-retinal and are proportional to the oscillator strengths. However, there is not any correspondence with the progression of the C11=C12 twist. Figure 8 shows a maximum value of the oscillator strength at 80° and a minimum at 10° of the dihedral angle C10-C11=C12-C13.

Fig. 5 Shapes of the LUMO (top) and HOMO (bottom) of the PSB-retinal conformers for several values of the dihedral angle C10-C11=C12-C13 when maintaining fixed the position of the four atoms and relaxing all the others. Isovalues for the MOs are 0.05 au

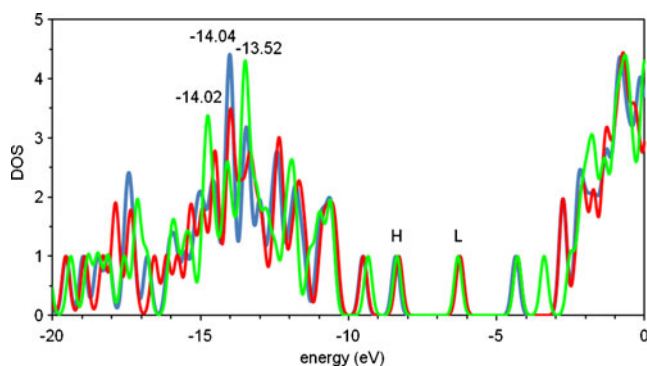0°   45°   90°   135°   180°

Fig. 6 Density of states (DOS) of the isomers 11-*cis*- (blue), transition state (green) and all-*trans*-PSB-retinal (red) at ground state. Occupied states are from the HOMO (H) to the left, and unoccupied states are from the LUMO to the right. Energies with the highest density of occupied molecular orbitals are shown for the three isomers. Regions where the blue curve is not shown are because of the strong overlap with the red curve

What is striking from this vertical excitation calculations is the similarity of the shapes of the singlet ground and first excited states of the molecule when the dihedral rotation keeps the four atoms fixed as indicated in Table 3. Rostov *et al*. [70] reported an inverted potential-energy curve for the first excited state of the retinal chromophore as a function of the rotation around the C11=C12 double bond. They find the minimum at 90° and the maxima near 0° and 180° using the CAM-B3LYP functional. For the excited state, they get a similar shape to the ground state potentials surface using the B3LYP functional. We decide to check why such a curve is different even when the B3PW91 is able to get the conic intersections of the C_2H_4 molecule (Fig. 9).

As expected, the B3PW91 yield the minimum at 90° for C_2H_4 excited state. Notice that most of the curves are symmetric with respect to 90° thus only this range is calculated. For these calculations (Fig. 9) we do not constrain the position of the four atoms making the fix

dihedral angle. Thus all atoms are free to relax, except the dihedral angle as indicated in Fig. 9. The smallest molecule (C_2H_4) yields the largest barrier of 2.99 eV. The next one correspond to $H_2C=HC-HC=CH-HC=CH_2$ (C_6H_8 in Fig. 9) the rotation through the central double bond yields a barrier of 1.44 eV almost half of the C_2H_4 excited state. We could say that as long as the molecule becomes larger the delocalization is larger and so the barrier decreases. We checked whether the effect of the N or the six member ring produces the inversion of the curve but we finally realize that the presence of the proton, to some extent, in the delocalized chain is what finally produces the inversion of curve. Perhaps the presence of the proton decreases even further the initially strong delocalization around the central double bond.

Needless to say, the calculations to obtain the potential surface of the first excited state are very time consuming and require a lot of care even when the molecules are relatively small. All coordinates are allowed to optimize freely at each point of the dihedral angle. This is different from what is done to obtain the results shown in Fig. 7, in which the four atoms making one of the dihedral angles are frozen allowing all other atoms to freely optimize the total energy. In the results of Fig. 9, the four atoms are not frozen but just the angle of two of their planes. One plane forces the two carbons of the double bond and the other two atoms connecting the first atom to be planar. The other plane includes the two atoms of the double bond and the two atoms connecting the second carbon of the double bond. The angle between these two planes with their four atoms each constrained to be planar is scanned from 0 to 90°. Although some of the curves are incomplete, the trends indicated by them, already provide information on their full behavior.

The NH_2 group attached to the end of the chain is where the extra proton is added. Even when we just add the HN,
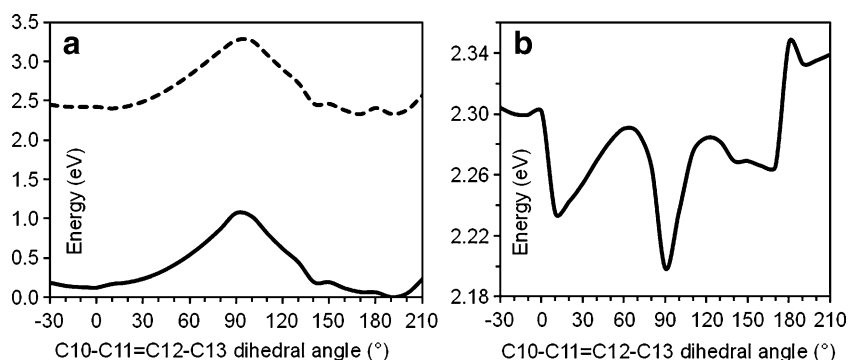

Fig. 7 (a) Relative energy of the isomerization at the ground state (S_0) and the first vertical exited state (S_v) of the protonated Schiff base retinal as compared to the all-*trans*-PSB-retinal energy. The difference between the S_v and S_0 states corresponds to the absorption energy. The energy of the reference corresponds to the energy of the all-*trans*-PSB-retinal at 190° (-834.40437 Ha). (b) Absorption energies of the

PSB-retinal conformers for the torsion around the C11=C12 bond. The ground state potential curve is obtained by optimization the isomers at every 10° keeping C10, C11, C12 and C13 atoms (Fig. 3) fixed. Then a single point TD-DFT is performed at each optimized geometry to get the vertical excitations

Table 3 First vertical excited state of the protonated Schiff base retinal isomers at several dihedral C10-C11=C12-C13 angles; the geometries are optimized for the ground state constraining the fours atoms at fixed distances of 1.434, 1.367, and 1.451 for the C10-C11, C11-C12, and C12-C13, respectively; and at angles of 130.8 and 132.2 for the C10-C11-C12 and C11-C12-C13, respectively. At each single point on the ground state surface the vertical excitation is calculated using TD-DFT yielding the absorption energy, main involved excited determinants with the highest occupied molecular orbital (H) and the lowest unoccupied molecular orbital (L), and oscillator strengths (f)

Dihedral angle (°)	Absorption energy (eV)	Involved MO transitions	f
-30	2.30	-0.1599(H-1→L)+0.5534(H→L)	1.2480
-20	2.30	-0.1651(H-1→L)+0.5546(H→L)	1.2084
-10	2.30	-0.1689(H-1→L)+0.5554(H→L)	1.1858
0	2.30	0.1704(H-1→L)+0.5557(H→L)	1.1816
10	2.23	0.1695(H-1→L)+0.5636(H→L)	1.0491
20	2.24	-0.1671(H-1→L)+0.5626(H→L)	1.0786
30	2.25	-0.1635(H-1→L)+0.5609(H→L)	1.1265
40	2.27	-0.1579(H-1→L)+0.5590(H→L)	1.1921
50	2.28	-0.1487(H-1→L)+0.5569(H→L)	1.2699
60	2.29	0.1330(H-1→L)+0.5551(H→L)	1.3558
70	2.29	0.1087(H-1→L)+0.5541(H→L)	1.4293
80	2.27	0.5538(H→L)	1.4616
90	2.20	0.5530(H→L)	1.3783
100	2.24	0.5557(H→L)	1.3220
110	2.28	-0.1118(H-1→L)+0.5562(H→L)	1.3596
120	2.28	-0.1367(H-1→L)+0.5565(H→L)	1.3600
130	2.28	-0.1527(H-1→L)+0.5571(H→L)	1.3436
140	2.27	-0.1673(H-1→L)+0.5579(H→L)	1.3308
150	2.27	-0.1673(H-1→L)+0.5579(H→L)	1.3309
160	2.27	-0.1697(H-1→L)+0.5578(H→L)	1.3391
170	2.27	0.1704(H-1→L)+0.5573(H→L)	1.3499
180	2.35	0.1710(H-1→L)+0.5588(H→L)	1.3015
190	2.33	-0.1663(H-1→L)+0.5508(H→L)	1.5091
200	2.34	-0.1630(H-1→L)+0.5508(H→L)	1.5087
210	2.34	0.1480(H-1→L)+0.5508(H→L)	1.5077

in order to have a neutral system, the maximum takes place at 0° or in the case of retinal ground, excited, and vertical states go into the positive side slightly. In all cases we try when the charge of the molecule is positive, the minimum at 90° disappears from the excited state surface and becomes a maximum.
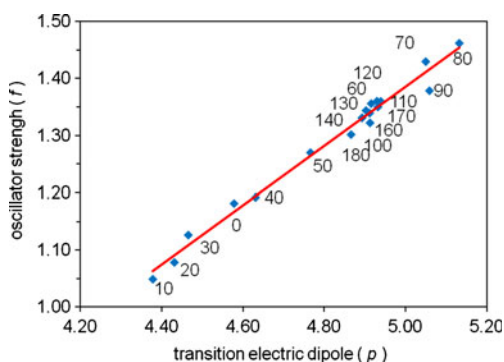

Fig. 8 Oscillator strength of the first vertical excited state versus transition electric dipole (with respect to the origin of coordinate) for the isomers of the PSB-retinal. Transition electric dipoles are in Debyes. C10-C11=C12-C13 for the case when the four atoms are kept fixed making the specific dihedral angles, which are shown in the curve in degrees. The regression equation is $f=0.5181p - 1.2048$ with a correlation factor of 0.9843

Therefore, a very special switching behavior is predictive from data in Fig. 9. The lowest rotational barrier (0.22 eV) takes place when retinal is neutral, in its excited state. The barrier increases sharply when the excited neutral goes to the ground state (2.15 eV). These values are in high contrast to the barrier of the retinal cation which is within 0.9 and 1.0 eV for the excited state and ~1.26 eV for the ground state. Thus rotation should occur when the molecule is neutral in its excited state, which is not the normal state of the molecule at dark conditions. A concerted reaction of photon absorption and deprotonation justifies the rotation starting from dark conditions and therefore the ejection of the proton after a photon with the right wavelength strikes the molecule.

As a comparison with shorter neutral molecules, the rotational barrier for the excited state (singlet) of C_2H_4 is 2.98 eV; it decreases for C_6H_8 to 1.44 eV and to 0.67 for $C_{12}NH_{14}$ and approaches zero as the molecule is longer but still neutral. For all cases the cations show larger barriers increasing in barrier as the molecules become shorter. The retinal shows barriers of 1.26 and 0.89 eV for the ground state singlet and excited singlet, respectively. Other cations such as $C_{15}NH_{20}$, $C_{12}NH_{15}$, and C_9NH_{12} yield barriers of 1.00, 0.88, and 2.15 eV, respectively; although a few more
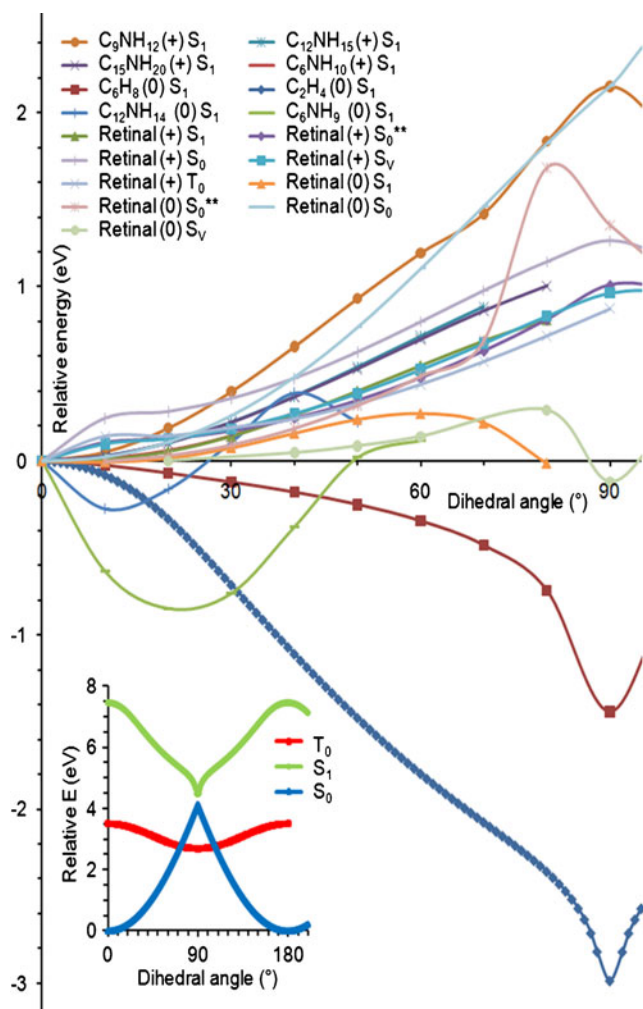
Fig. 9 Potential energy surface of retinal and other related molecules around the C=C bonds, including ground and first singlet excited states as well as neutral and protonated states. All energies are relative with respect to their energy at 0°. S_1 and S_0 are calculated by rotation of the central C=C double bond scanning the angle between two planes containing the two double-bonded atoms, where one plane contains also the two other atoms connected to the first carbon of the double bond, and the second plane contains the two atoms connected to the second carbon. S_v and S_0^{**} are calculated by freezing the four atoms which make the dihedral angle allowing all other atoms to freely optimize the total. The inset shows the S_0, S_1, and T_0 of C_2H_4 where the three curves are relative to the ground state singlet at 0°

points are needed to complete the first two curves, their qualitative behavior is what really has importance for this group. The calculations on smaller molecules may certainly mislead any prediction of the behavior of retinal.

Figure 10 shows that all conformers absorb at green visible region (577-492 nm). However, at violet region (455 nm-390 nm), the transition state of the PSB-retinal (90° dihedral angle C10-C11=C12-C13) lacks absorption. The new deprotonated state (all-SB-trans-retinal) absorbs in the violet region with higher intensity compared with the all trans-PSB-retinal (Table 4), in agreement with [71]. The
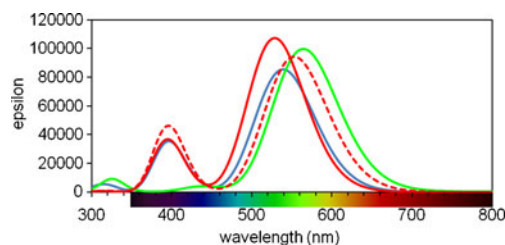

Fig. 10 Visible spectra for the *cis*-PSB-retinal (blue), TS-PSB-retinal (green), *trans*-PSB-retinal (red) and *trans*-BS-retinal (dashed red)

absorption maximum calculated for the *cis*-PSB-retinal (540 nm) by TD-B3PW91/6-31G(*d*) overestimates the experimental value in the rhodopsin protein (500 nm) [72] due perhaps to absence of the counterion aminoacid, as explained in [73].

Conclusions

We find that the retinal molecule has a higher probability to rotate when its charge state is zero and it is in its excited state; barrier is ~0.22 eV as compared to the barrier for the protonated molecule which is in the range of 0.9 eV. We conclude that rotation takes place in the deprotonated retinal. The addition of a proton creates a barrier implying a switching behavior of retinal that might be useful for several applications in molecular electronics. The interaction of light with 11-*cis*-PSB-retinal causes configurational changes and favors its deprotonation at the N-Schiff base, incrementing the absorption of light at the violet region. Thus, we conclude that the absorption energy activates the deprotonation of the chromophore, regardless of the absence in the calculation of the counterion aminoacids. The transition state of the photoisomerization from 11-*cis*- PSB-retinal to all-*trans*-PSB-retinal occurs at 90° dihedral C10-C11=C12-C13, which does not absorb around 400 nm. However, the absorption energy depends on the configuration and the protonated state of the retinal. During isomerization, there is a rearrangement of electron density due to the rotation around the C11=C12 bond. Since under light absorption, isomerization and deprotonation occur simultaneously, it is appealing to explore the likelihood of

Table 4 Energy absorption of the protonated 11-*cis*-, transition state and all-*trans*-, and the unprotonated all-*trans*-Schiff base retinal

	Compound	Maximum energy absorption (nm)	Second region of energy absorption (nm)
1	*11-cis*-PSB-retinal	540	400
2	TS-PSB-retinal	560	-
3	all-*trans*-PSB-retinal	520	400
4	all-*trans*-SB-retinal	550	400

using light sensitive molecules as molecular logical circuits to develop photo-electro-sensors or photo-devices.

References

1. Trushin MV (2004) Light-mediated "conversation" among micro-organisms. Microbiol Res 159:1–10

2. Fels D (2009) Cellular communication through light. PLoS ONE 4:1–8

3. Jékely G (2009) Evolution of phototaxis. Phil Trans R Soc B 364:2795–2808

4. Sytina OA, Heyes DJ, Hunter CN, Groot ML (2009) Ultrafast catalytic processes and conformational changes in the light-driven enzyme protochlorophyllide oxidoreductase (POR). Biochem Soc Trans 37:387–391

5. Rangel NL, Williams KS, Seminario JM (2009) Light-Activated Molecular Conductivity in the Photoreactions of Vitamin D3. J Phys Chem A 113:6740–6744

6. Kim TY, Uji-i H, Möller M, Muls B, Hofkens J, Alexiev U (2009) Monitoring the Interaction of a Single G-Protein Key Binding Site with Rhodopsin Disk Membranes upon Light Activation. Biochemistry 48

7. Gascón JA, Sproviero EM, Batista VS (2006) Computational studies of the primary phototransduction event in visual rhodopsin. Acc Chem Res 39:184–193

8. Kakitani T, Kakitani H (1975) Molecular mechanism for the initial process of visual excitation. I. Model of photoisomerization in rhodopsin and its theoretical basis by quantum mechanical calculation of adiabatic potential. J Phys Soc Jpn 38:1455–1463

9. Warshel A (1976) Bicycle-pedal model for the first step in the vision process. Nature 260:679–683

10. Liu RSH, Hammond GS (2000) The case of medium-dependent dual mechanisms for photoisomerization: One-bond-flip and Hula-Twist. PNAS 97:11153–11158

11. Yamada A, Yamato T, Kakitani T, Yamamoto S (2002) Analysis of Cis-Trans Photoisomerization Mechanism of Rhodopsin Based on the Tertiary Structure of Rhodopsin. J Photosci 9:51–54

12. Frutos LM, Andruniów T, Santoro F, Ferreé N, Olivucci M (2007) Tracking the excited-state time evolution of the visual pigment with multiconfigurational quantum chemistry. PNAS 104:7764–7769

13. Schapiro I, Weingart O, Buss V (2009) Bycicle-pedal in a rhodopsin chromophore model. J Am Chem Soc 131:16–17

14. Jardón-Valadez E, Bondar AN, Tobias DJ (2009) Dynamics of internal water molecules in squid rhodopsin. Biophys J 96:2572–2576

15. Craddock TJA, Beauchemin C, Tucszynski JA (2009) Information processing mechanisms in microtubules at physiological temperature: Model predctions for experimetal tests. BioSystems 97:28–34

16. Palczewski K, Kumasaka T, Hori T, Behnke CA, Motoshima H, Fox BA, Trong IL, Teller DC, Okada T, Stenkamp RE, Yamamoto M, Miyano M (2000) Crystal structure of rhodopsin: A G protein-coupled receptor. Science 289:739–745

17. Hornak V, Ahuja S, Eilers M, Goncalves JA, Sheves M, Reeves PJ, Smith SO (2010) Light activation of rhodopsin: insights from molecular dynamics simulations guided by solid-state NMR distance restraints. J Mol Biol 396:510–527

18. Crocker E, Eilers M, Ahuja S, Hornak V, Hirshfeld A, Sheves M, Smith SO (2006) Location of Trp265 in Metarhodopsin II:

19. Patel AB, Crocker E, Eilers M, Hirshfeld A, Sheves M, Smith SO (2004) Coupling of retinal isomerization to the activation of rhodopsin. PNAS 101:10048–10053

20. Yan EC, Kazmin MA, Ganim Z, Hou JM, Pan D, Chang BS, Sakmar TP, Mathies RA (2003) Retinal counterion switch in the photoactivation of the G protein-coupled receptor rhodopsin. Proc Natl Acad Sci 100:9105–9107

21. Smitienko OA, Mozgovaya MN, Shelaev IV, Gostev FE, Feldman TB, Nadtochenko VA, Sarkisov OM, Ostrovsky MA (2010) Femtosecond formation dynamics of primary photoproducts of visual pigment rhodopsin. Biochemistry 75:34–45

22. Kukumura P, McCamant DW, Yoon S, Wandschneider DB, Mathies RA (2005) Structural observation of the primary isomerization in vision with femtosecond-stimulated Raman. Science 310:1006–1009

23. Estevez ME, Kolesnikov AV, Ala-Laurila P, Crouch RK, Govardovskii VI, Cornwall MC (2009) The 9-methy group of retinal is essential for rapid Meta II decay and phototransduction quenching n red cones. J Gen Physiol 134:137–150

24. Vassilieva-Vashakmadze NS, Gakhokidze RA, Gakhokidze AR (2008) Mechanism of Photoisomerization of the Rhodopsin Chromophore. Biochemistry 73:730–732

25. Vogel R, Mahalingam M, Lüdeke S, Huber T, Siebert F, Sakmar TP (2008) Functional role of the "Ionic Lock"- An interhelical hydrogen-bond netwerok in Family a heptahelical rcepetors. J Mol Biol 380:648–655

26. Isin B, Schulten K, Tajkhorshid E, Bahar I (2008) Mechanism of signal propagation upon retinal isomerization: insights from molecular dynamics simulations of rhodopsin restrained by normal modes. Biophys J 95:789–803

27. Angel TE, Chance MR, Palczewski K (2009) Conserved waters mediate structural and functional activation of family A (rhodopsin-like) G-protein-coupled receptors. PNAS 106:8555–8560

28. Seminario JM, Yan L, Ma Y (2005) Transmission of vibronic signals in molecular circuits. J Phys Chem A 109:9712–9715

29. Seminario JM, Yan L, Ma Y (2005) Scenarios for molecular-level signal processing. Proc IEEE 93:753–1764

30. Seminario JM, Yan L (2007) Cascade configuration of logical gates processing information encoded in molecular potentials. Int J Quantum Chem 107:754–761

31. Seminario JM, Yan L, Ma Y (2006) Encoding and Transport of Information in Molecular and Biomolecular Systems. IEEE Transact Nanotechnol 5:436–440

32. Salazar-Salinas K, Seminario JM (2010) Energetics and vibronics analyses of the enzymatic coupled electron-proton transfer from nfsa nitroreductase to trinitrotoluene. IEEE Transact Nanotechnol 9:543–553

33. Salazar PF, Seminario JM (2008) Identifying receptor-ligand interactions through an ab initio approach. J Phys Chem B 112:1290–1292

34. Cristancho D, Seminario JM (2010) Polypeptides in alpha-helix conformation perform as diodes. J Chem Phys 132:065102-1–065102-5

35. Kohn W (1996) Density functional and density matrix method scaling linearly with the number of atoms. Phys Rev Lett 76:3168–3171

36. Kohn W, Sham LJ (1965) Self-consistent equations including exchange and correlation effects. Phys Rev 140:A1133–A1138

37. Kohn W, Sham LJ (1965) Quantum density oscillations in an inhomogeneous electron gas. Phys Rev 137:A1697–A1705

38. Luo Y, Gelmont BL, Woolard DL (2006) In: Seminario JM (ed) "Bio-molecular devices for terahertz frequency sensing," in molecular and nano electronics: analysis, design and simulation, vol 17. Elsevier, Amsterdam, pp 96–140

Implictions for the Activation mehanism of the visual receptor rhodopsin. J Mol Biol 357:163–172

39. Frisch MJ, Trucks GW, Schlegel HB, Scuseria GE, Robb MA, Cheeseman JR, Montgomery JA, Vreven TJ, Kudin KN, Burant JC, Millam JM, Iyengar SS, Tomasi J, Barone V, Mennucci B, Cossi M, Scalmani G, Rega N, Petersson GA, Nakatsuji H, Hada M, Ehara M, Toyota K, Fukuda R, Hasegawa J, Ishida M, Nakajima T, Honda Y, Kitao O, Nakai H, Klene M, Li X, Knox JE, Hratchian HP, Cross JB, Adamo C, Jaramillo J, Gomperts R, Stratmann RE, Yazyev O, Austin AJ, Cammi R, Pomelli C, Ochterski JW, Ayala PY, Morokuma K, Voth GA, Salvador P, Dannenberg JJ, Zakrzewski VG, Dapprich S, Daniels AD, Strain MC, Farkas O, Malick DK, Rabuck AD, Raghavachari K, Foresman JB, Ortiz JV, Cui Q, Baboul AG, Clifford S, Cioslowski J, Stefanov BB, Liu G, Liashenko A, Piskorz P, Komaromi I, Martin RL, Fox DJ, Keith T, Al-Laham MA, Peng CY, Nanayakkara A, Challacombe M, Gill PMW, Johnson B, Chen W, Wong MW, Gonzalez C, Pople JA (2003) Gaussian-2003, Revision C.2. Gaussian Inc, Pittsburgh, PA

40. Frisch MJ, Trucks GW, Schlegel HB, Scuseria GE, Robb MA, Cheeseman JR, Scalmani G, Barone V, Mennucci B, Petersson GA, Nakatsuji H, Caricato M, Li X, Hratchian HP, Izmaylov AF, Bloino J, Zheng G, Sonnenberg JL, Hada M, Ehara M, Toyota K, Fukuda R, Hasegawa J, Ishida M, Nakajima T, Honda Y, Kitao O, Nakai H, Vreven T, Montgomery JA Jr, Peralta JE, Ogliaro F, Bearpark M, Heyd JJ, Brothers E, Kudin KN, Staroverov VN, Kobayashi R, Normand J, Raghavachari K, Rendell A, Burant JC, Iyengar SS, Tomasi J, Cossi M, Rega N, Millam JM, Klene M, Knox JE, Cross JB, Bakken V, Adamo C, Jaramillo J, Gomperts R, Stratmann RE, Yazyev O, Austin AJ, Cammi R, Pomelli C, Ochterski JW, Martin RL, Morokuma K, Zakrzewski VG, Voth GA, Salvador P, Dannenberg JJ, Dapprich S, Daniels AD, Farkas O, Foresman JB, Ortiz JV, Cioslowski J, Fox DJ (2009) Gaussian 09, Revision A.02. Gaussian Inc, Wallingford, CT

41. Becke AD (1993) A new mixing of Hartree-Fock and local density-functional theories. J Chem Phys 98:1372–1377

42. Perdew JP, Chevary JA, Vosko SH, Jackson KA, Pederson MR, Singh DJ, Fiolhais C (1992) Atoms, molecules, solids, and surfaces: applications of the generalized gradient approximation for exchange and correlation. Phys Rev B 46:6671–6687

43. Perdew JP (1986) Density-functional approximation for the correlation energy of the inhomogeneous electron gas. Phys Rev B 33:8822–8824

44. Hariharan PC, Pople JA (1973) The influence of polarization functions on molecular orbital hydrogenation energies. Theor Chim Acta 28:213–222

45. Hehre WJ, Dithfield R, Pople JA (1972) Self-Consistent Molecular Orbital Methods. XII. Further Extensions of Gaussian-Type Basis Set for Use in Molecular Orbital Studies of Organic Molecules. J Chem Phys 56:2257–2261

46. Rassolov VA, Ratner MA, Pople JA, Redfern PC, Curtiss LA (2001) 6-31 G* basis set for third-row atoms. J Comput Chem 22:976–984

47. Rangel NL, Seminario JM (2006) Molecular electrostatic potential devices on graphite and silicon surfaces. J Phys Chem A 110:12298–12302

48. Yan L, Ma Y, Seminario JM (2006) Terahertz signal transmission in molecular systems. International J High Speed Electron Syst 16:669–675

49. Yan L, Ma Y, Seminario JM (2006) Encoding information using molecular vibronics. J Nanosci Nanotechnol 6:1–10

50. Seminario JM, Yan L, Ma Y (2005) Nano-Detectors Using Molecular Circuits Operating at THz Frequencies. Proc SPIE 5995:59950R-1–59950R-15

51. Seminario JM, Yan L, Ma Y (2005) Encoding and transport of information in molecular and biomolecular systems. Proc 2005 5th IEEE Conf Nanotechnol 1:65–68

52. Seminario JM, de la Cruz C, Derosa PA, Yan L (2004) Nanometer-size conducting and insulating molecular devices. J Phys Chem B 108:17879–17885

53. Derosa PA, Guda S, Seminario JM (2003) A programmable molecular diode driven by charge-induced conformational changes. J Am Chem Soc 125:14240–14241

54. Wang K, Rangel NL, Kundu S, Sotelo JC, Tovar RM, Seminario JM, Liang H (2009) Switchable molecular conductivity. J Am Chem Soc 131:10447–10451

55. Sotelo JC, Seminario JM (2007) Biatomic substrates for bulk-molecule interfaces: The PtCo-oxygen interface. J Chem Phys 127:244706-1–244706-13

56. Sotelo JC, Seminario JM (2008) Local reactivity of O2 with Pt3 on Co3Pt and related backgrounds. J Chem Phys 128:204701-1–204701-11

57. Derosa PA, Seminario JM, Balbuena PB (2001) Properties of small bimetallic Ni-Cu clusters. J Phys Chem A 105:7917–7925

58. Habibollahzadeh D, Grodzicki M, Seminario JM, Politzer P (1991) Computational study of the concerted gas-phase triple dissociations of 1, 3, 5-Triazacyclohexane and its 1, 3, 5-Trinitro derivative (RDX). J Phys Chem 95:7699–7702

59. Politzer P, Seminario JM (1993) Computational study of the structure of dinitraminic acid, HN(NO2)2 and the energetics of some possible decomposition steps. Chem Phys Lett 216:348–352

60. Seminario JM, Concha MC, Politzer P (1995) A density functional/molecular dynamics of the structure of liquid nitro-methane. J Chem Phys 102:8281–8282

61. Politzer P, Seminario JM (1993) Energy changes associated with some decomposition steps of 1, 3, 3-trinitroazetidine - a nonlocal density-functional study. Chem Phys Lett 207:27–30

62. Politzer P, Seminario J, Bolduc P (1989) A proposed interpretation of the destabilizing effect of hydroxyl-groups on nitroaromatic molecules. Chem Phys Lett 158:463–469

63. Seminario JM, Concha MC, Politzer P (1992) Calculated structures and relative stabilities of furoxan, some 1, 2 dinitroso-ethylenes and other isomers. J Comput Chem 13:177–182

64. Murray J, Redfern P, Seminario J, Politzer P (1990) Anomalous energy effects in some aliphatic and Alicyclic Aza systems and their nitro-derivatives. J Phys Chem A 94:2320–2323

65. Salazar PF, Seminario JM (2007) Simple energy corrections for precise atomization energies of CHON molecules. J Phys Chem A 111:11160–11165

66. Send R, Sundholm D (2007) Stairway to the conical intersection: A computational study of the retinal isomerization. J Phys Chem A 111:8766–8773

67. Muñoz-Loza A, Galván IF, Aguilar MA, Martín ME (2008) Retinal models: Comparison electronic absorption spectra in the gas phase and in methanol solution. J Phys Chem B 112:8815–8823

68. Wanko M, Hoffmann M, Strodel P, Koslowski A, Thiel W, Neese F, Frauenheim T, Elstner M (2005) Calculating absorption shifts for retinal proteins: computational challenges. J Phys Chem B 109:3606–3615

69. Andruniów T, Ferré N, Olivucci M (2004) Structure, initial excited-state relaxation, and energy storage of rhodopsin resolved at the multiconfigurational perturbation theory level. PNAS 101:17908–17913

70. Rostov IV, Amos RD, Kobayashi R, Scalmani G, Frisch MJ (2010) Studies of the ground and excited-state surfaces of the retinal chromophore using CAM-B3LYP. J Phys Chem B 114:5547–5555

71. Altun A, Yokoyama S, Morokuma K (2008) Mechanism of spectral tuning going from retinal in vacuo to bovine rhodopsin and its mutants: multireference ab initio quantum mechanics/molecular mechanics studies. J Phys Chem B 112:16883–16890

72. Sakmar TP, Franke RR, Khorana HG (1989) Glutamic acid-113 serves as the retinylidine Schiff base counterion in bovine rhodopsine. Proc Natl Acad Sci 86:8309–8313

73. Bravaya K, Bochenkova A, Granovsky A, Nemukhin A (2007) An opsin shift in rhodopsin: retinal S0→S1 excitation in protein, in solution, and in gas phase. J Am Chem Soc 129:13035–13042